Transactions in GIS

WILEY

Transactions in GIS

RESEARCH ARTICLE OPEN ACCESS

Evaluating the Enhanced Bathtub Model for Coastal Flood Risk Assessment in Table Bay, South Africa

Melanie Lück-Vogel[1,2] | Frederick Joshua van Coller[1] | Lauren Lyn Williams[3]

[1]Department of Geography and Environmental Studies, Stellenbosch University, Stellenbosch, South Africa | [2]Coastal Systems & Earth Observation Research Group, CSIR, Stellenbosch, South Africa | [3]National Department of Forestry, FIsheries and the Environment, Department of Forestry, Fisheries and the Environment, Cape Town, South Africa

Correspondence: Melanie Lück-Vogel (mluckvogel@csir.co.za; mluckvogel@gmail.com)

Received: 20 March 2024 | **Revised:** 28 August 2024 | **Accepted:** 9 October 2024

Funding: This study was supported by South African Parliamentary (Grant P1ECS01).

Keywords: coastal flooding | enhanced bathtub model | GIS modeling | inundation | South Africa

ABSTRACT

Coastal zones are susceptible to increasing pressures from urban development and natural hazards, such as storm events, climate change, and rising sea levels. The GIS-based enhanced bathtub model (eBTM) enables the identification of areas at risk of flooding as a baseline for disaster management and coastal adaptation. This study aims to establish the methodological robustness of the eBTM for coastal flood modeling, by analyzing eight sites flooded during a recent storm event in Table Bay, Cape Town by comparing eBTM outputs with observed flood extent data collected after the storm. The validation showed that for 74% of the 332 validation points the spatial modeling error was < 6 m and for 56% below 3 m. The root mean square error for the model was 4.88 m, indicating an acceptable level of accuracy of the eBTM outputs for coastal risk assessments where more sophisticated models are unavailable.

1 | Introduction

Coastal zones present a dynamic interface between land and sea and are subject to the influences of both natural processes and human activities (Crossland et al. 2005; Rutledge et al. 2022; Saravanan, Parthasarathy, and Vishnuprasath 2019), housing approximately 44% of the world population (UN Atlas of the Oceans 2016). Beyond their demographic significance, coastal regions provide crucial economic and livelihood resources. Coasts encompass a rich tapestry of ecosystems, spanning from sandy beaches to cliffs and wetlands, hosting an abundant biodiversity (Baztan et al. 2015; Williams, Dodd, and Gohn 1995; Skowno et al. 2019). The escalating trends in development and associated pressures on coasts are a cause for concern, threatening natural ecosystem functioning and putting an increasing amount of people, infrastructure and livelihoods at risk of damage from natural hazards (Goschen 2011; Wepener and Degger 2019). Climate change, predicted to lead to increasingly frequent and intense storm events, sea level rise and a potential shift in weather patterns, is exacerbating existing hazards and risks in the coastal zone, specifically the impact of coastal flooding and erosion (Intergovernmental Panel on Climate Change [IPCC] 2019, 2021, 2022; Sink et al. 2012).

In South Africa, in 2015 about 466,148 people were living in coastal areas between 0 and 10 m above sea level, constituting about 8.5% of the country's total population (CIESIN et al. 2024). South Africa's 3100 km long coastline borders the southern Atlantic and the Indian oceans, both regular sources of storm events already leading to significant economic losses (Dube, Nhamo, and Chikodzi 2022). According to Theron and Rossouw (2008) the densely populated coasts of the Northern False Bay, Table Bay (both within the City of Cape Town), Saldanha Bay, the South Cape coast, Mossel Bay, Port Elizabeth, and parts of the KwaZulu-Natal province, stand out as particularly vulnerable to the impacts of climate change-induced

flooding and erosion in South Africa. Given their high coastal population density, the City of Cape Town and the province of KwaZulu-Natal experienced the highest number of flood and storm-related disasters between 1980 and 2022 on South Africa's coast (Bopape et al. 2024).

South Africa in general has limited capacity for implementing complex hydrodynamic models to provide coastal flood risk predictions as baseline information for coastal spatial planning, disaster preparedness and for climate change adaptation. In response, Williams (2020) developed the GIS-based enhanced bathtub model (eBTM) to address this gap. GIS-based bathtub models have been used in many studies for determining areas at risk of flooding in the context of sea level rise (e.g., Li, Grady, and Peterson 2014; Fitchett, Grant, and Hoogendoom 2016; Almaliki et al. 2023; Carneiro-Barros et al. 2023). The eBTM differs from the common simple bathtub model by introducing hydrological connectivity, thereby minimizing false positives for disconnected areas, and also considering slope and surface roughness (or complexity) as factors for water distribution (Williams 2020). However, being a GIS-based model, there are known limitations such as its inability to incorporate spatiotemporally dynamic data such as wind speed and wave direction (Williams and Lück-Vogel 2020).

The eBTM is an explanatory model, developed for estimating coastal flood extent under circumstances where more sophisticated modeling technology, such as hydrodynamic modeling, or the required input data are not available. The eBTM therefore fills an important methodological gap in data and technology scarce countries such as South Africa. Subsequently, the eBTM has been applied by Kouakou et al. (2023) to model flooding by sea level rise in Côte d'Ivoire, Nguyen and Kuleshov (2023) in Australia and Jennath and Paul (2024) in India. However, these studies do not undertake any rigorous localized validation of their model results relative to previous flood events.

The quality of model input data is known to affect the model output (Gesch 2009; Quinn et al. 2014; Vousdoukas et al. 2018; Rohmer et al. 2021; Williams and Lück-Vogel 2022). However, the overall robustness of coastal flood and vulnerability models, that is, the performance across different areas and different environments, is becoming an increasing focus of research as modeling outputs are increasingly used to inform adaptation with real-world cost implications (Clasing et al 2023). The establishment of the methodological robustness of the eBTM model is therefore critical if the outputs are used as baseline for effective coastal protection and climate adaptation action.

This study assesses the robustness of the eBTM model using the same topographic input data as per Williams and Lück-Vogel (2022) and the wave run-up heights that resulted in a recent flooding event that occurred in Table Bay, Cape Town on 16 September 2023. The performance of the model was assessed using ground validation data collected on eight sites in Table Bay immediately after the storm event. The outcomes of this validation therefore provide insights into the applicability of the eBTM for planning purposes.

2 | Data and Methods

2.1 | Study Area

The study area selected for this research was Table Bay on the coast of the City of Cape Town, at the southwestern tip of South Africa (Figure 1). Table Bay's coastline of about 40 km length encompasses sandy beaches, rocky shores, and coastal wetlands. Its urban coastal landscape is complex, blending residential, commercial, and industrial areas with vital infrastructure such as a major port, roads, bridges, and utilities, on a diverse geomorphology. The climate is Mediterranean, characterized by hot, dry summers and cool, wet winters, with strong southeasterly winds in summer, and northwesterly winds in winter. The predominant wave direction is from the southwest (Figure 1).

Table Bay was selected due to its history of past flooding events. The urgency for accurate flood modeling in this region is underscored by the occurrence of four major floods within a 4-month period in 2023, occurring on 14 June 2023, 16 September 2023, 24 September 2023, and 21 October 2023. This study focusses on the storm that occurred on 16 September 2023. On 16 September 2023, the South African Weather Service issued a critical Orange Level 5 Alert in response to a powerful storm approaching from the South Atlantic which resulted in heavy winds and rainfall, a storm surge, compounded by the occurrence of equinox spring tides. The two virtual buoys VT03 and VT05 located in Table Bay (Figure 1) measured significant wave heights (HM_0) of 3.82 and 5.26 m, respectively, during the peak storm (Figure 2).

The average wind speed, as measured at the Cape Town Port's entrance during the peak storm event, was around 10 m/s with maximum winds speeds reaching about 18 m/s and a general wind direction of east-southeast (around 250°). This event provided a chance to collect sufficient ocean and ground data at eight distinct sites in Table Bay as input for the eBTM and to validate its outputs. The eight sites were selected based on safe accessibility for data capturing. The sites, listed from North to South, are Melkbosstrand North, Melkbosstrand South, Bloubergstrand, Lagoon Beach, Mouille Point, Sea Point, Camps Bay, and Bakoven Beach (Figure 1a–h). All sites have experienced coastal flooding in the past. Each subarea was considered in terms of its morphology (see Appendix A), leading to a broad classification of the site, as described in Table 1.

2.2 | Input Data

To run the eBTM, the following input data needed to be sourced or created: a high-resolution elevation model, a reference coastline, local wave heights, and the land surface roughness.

2.2.1 | High-Resolution Topographic Data

Inundation modeling needs accurate high-resolution topographic data (Gesch 2009; Williams and Lück-Vogel 2020, 2022). For this study, LiDAR data were made available by the City of Cape Town in the LAS point file format with a point density of about 10 points per m^2. For the southern study area between Bakoven Beach and Mouille Point, relatively recent

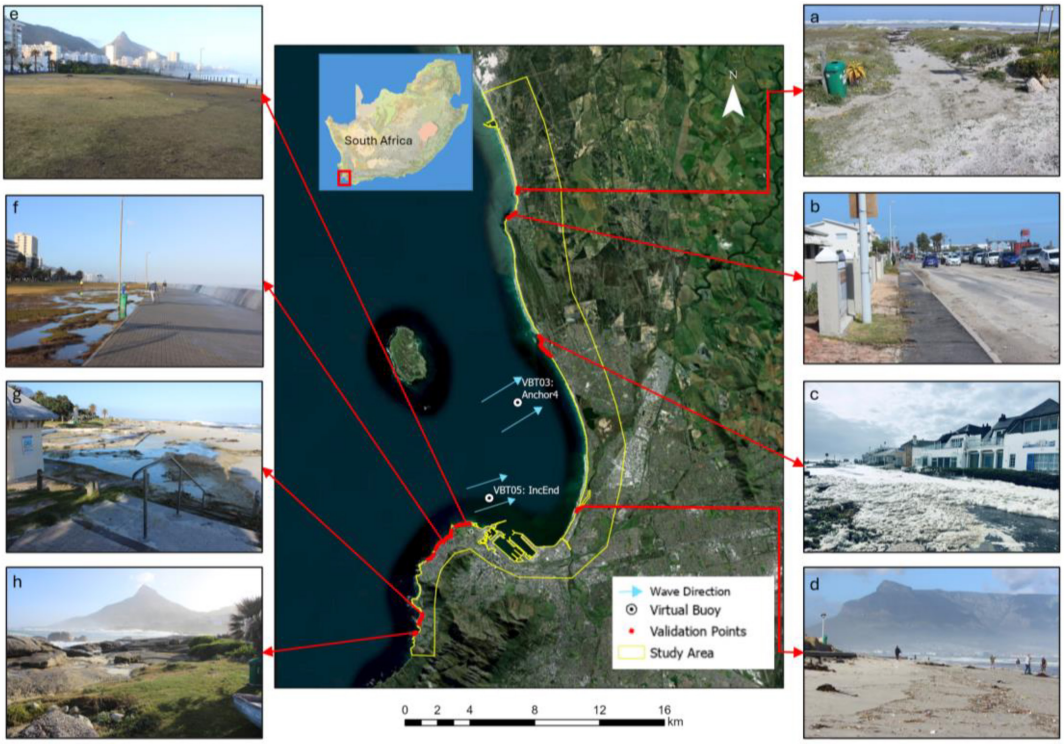

FIGURE 1 | Location of study subareas in Table Bay with poststorm impressions. (a) Melkbosstrand North, (b) Melkbosstrand South, (c) Bloubergstrand, (d) Lagoon Beach, (e) Mouille Point, (f) Sea Point, (g) Camps Bay, and (h) Bakoven Beach.

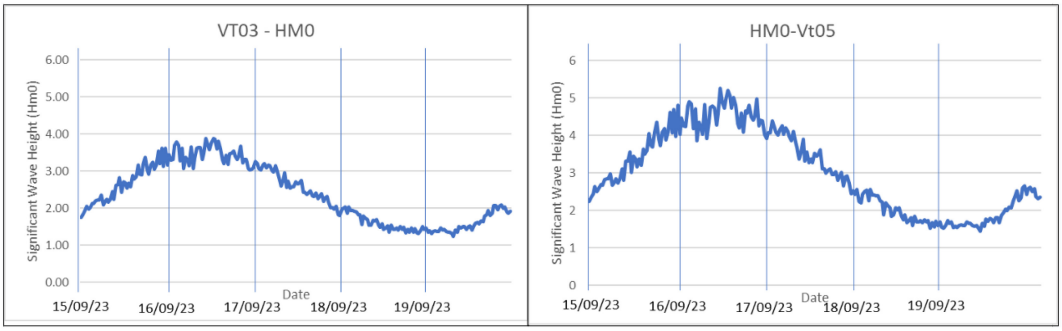

FIGURE 2 | Significant wave height of the virtual buoys over the storm period.

TABLE 1 | Classification of study sites subareas.

Study subarea	Morphology
a Melkbosstrand North	Shallow wide sandy shore + reef
b Melkbosstrand South	Shallow narrow sandy shore
c Bloubergstrand	Shallow narrow sandy shore + reef
d Lagoon Beach	Shallow narrow sandy shore with estuary mouth
e Mouille Point	Highly modified shore + reef
f Sea Point	Highly modified shore + reef
g Camps Bay	Shallow wide sandy shore
h Bakoven Beach	Steep rocky shore

data from February 2023 were available. For the study area further north, only LiDAR data acquired in November 2021 were available.

To generate a digital surface model (DSM) of the study area, the first-return points of the LiDAR datasets were used. The DSM, in contrast to a digital terrain model, accounts for the presence of

vegetation and manmade structures, both of which can significantly affect the flow of water during flooding events (Williams and Lück-Vogel 2020). The resulting DSM had a horizontal resolution of 1 × 1 m and a vertical resolution of 0.01 m. The projection was Transverse Mercator Lo19, with South African Land Leveling Datum as vertical datum.

2.2.2 | Reference Coastline

The eBTM requires a polyline water source as input which marks the starting point for the model's execution. This line is typically represented by the coastline (Williams 2020). A coastline polyline shapefile (ESRI GIS proprietary data format) at the required spatial and temporal accuracy was digitized manually from recent high-resolution Google Earth imagery, using the visible wetline as reference. It was confirmed that the resulting reference coastline intersects the LiDAR-derived DSM for proper model execution.

2.2.3 | Ground Data on Flood Extent

The morning after the storm, that is, 17 September 2023, field data were collected in the form of georeferenced photographs for accessible study subareas, documenting the extent of the flooding. Figure 1 provides examples of these photographs. The photographs were used to locate and mark the maximum flood extent visible as wet and/or debris line in the photographs, resulting in 340 data points. To correct for potential location errors caused by the oblique field photographs, high-resolution recent Google Earth imagery was used to better pinpoint the location of the wetlines.

2.2.4 | Wave Run-Up Height

"Wave run-up" refers to the vertical elevation attained by the leading edge of a wave as it advances up a shoreline, measured relative to the still water line (Roux 2015). The first approach for assessing wave run-up was using the measured wave heights at the two virtual buoys in Table Bay (see Figure 1). However, these data turned out not to be representative for the complex coastline of Table Bay with an interplay of refractive and dissipative and steep rocky and flat sandy shores, which resulted in very different wave run-up on the study subareas. It was therefore decided to use the DSM elevation at one randomly selected ground-recorded floodline point within each subarea as wave-run-up input for the eBTM model. The resulting wave run-up heights for each subarea, ranging from 2.92 m at Melkbosstrand to 5.59 m at Mouille Point, are illustrated in Figure 3.

2.2.5 | Roughness Coefficient

The roughness or smoothness of the terrain influences water movement, with water moving faster and further on smooth

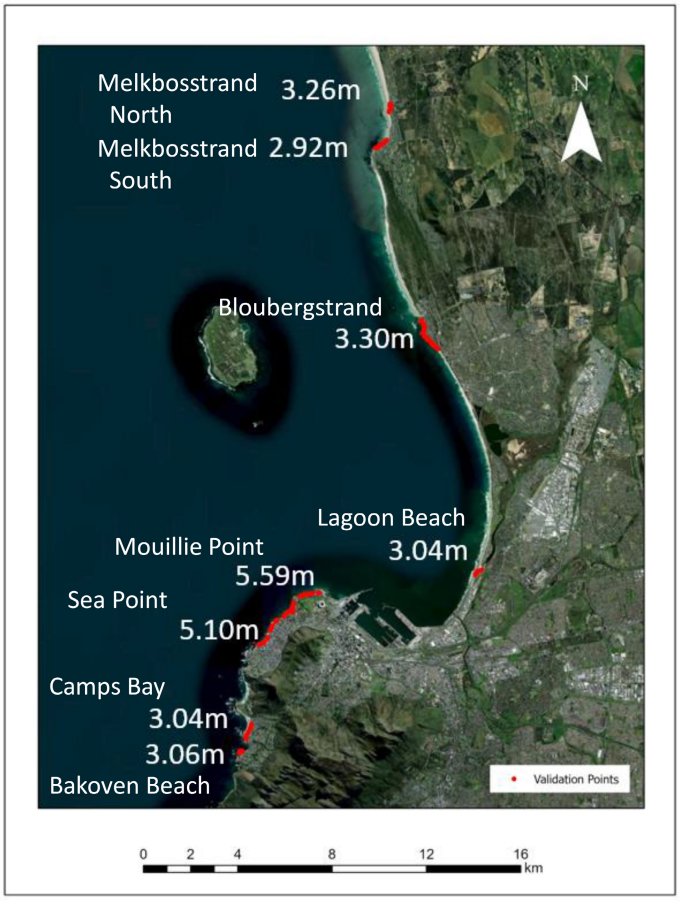

FIGURE 3 | Wave run-up height per subarea with location of ground validation data.

surfaces such as sand or tar than on rough surfaces such as vegetated areas or coarse rock revetments. In the eBTM, the roughness coefficient relates more to a subjective assessment of the surface complexity, rather than conforming to the Manning roughness coefficient used in hydrodynamic models. The roughness data range with values between 0 (indicative of hydraulically very rough surfaces) and 1 (representative of very smooth surfaces) allows the user to choose a roughness value most representative across the study area (Williams 2020). As the sites affected by flooding in the study area primarily consisted of smooth sandy terrain or lawns and tarred or paved urban developments, a roughness coefficient value of 1 was used for all model runs.

2.3 | Flood Modeling

The eBTM model was executed for each of the eight sites separately, given the substantially different observed wave run-up heights between the areas (Figure 3). The model was obtained as part of a Toolbox (ArcCoastTools [https://catalogue.saeon.ac.za/records/10.15493/DEFF.10000001]) and added as such to ArcMap 10.4.1, under inclusion of the Spatial Analyst extension. The LiDAR-derived high-resolution elevation model, the digitized reference coastline, the respective local wave run-up established for the flood event that occurred on 16 September 2023 and the land surface roughness were used as input data for each area.

The first processing step in the GIS-based eBTM model is the elimination of all areas in the DSM which are lying higher than the subarea-specific input water level elevation as those areas are assumed to be safe from flooding. For the area lower than the input water level height, the cost-distance module examines the slope angle of the land to understand how water might flow and calculates the cost of moving through various areas. This information is combined to determine the progression of inundation from the coastline, considering pathways that facilitate water movement and the potentially dampening effect of the local surface roughness. Unconnected low-lying areas will be excluded from short-term flooding relating to flooding, which is one of the major advantages of the eBTM compared to the commonly used standard bathtub model which only considers topographic elevation but not hydrological connectivity. The output of the eBTM is a binary flood mask showing the final flood extent. Inundation depth is also generated by the eBTM model but was not used for this study (Williams and Lück-Vogel 2020).

2.4 | Accuracy Assessment

For an estimation of the accuracy of the eBTM outputs, the distance of the modeled floodlines to the respective nearest validation point was measured, using the Near Tool in ArcGIS Pro. The root mean square error (RMSE) of these distances was calculated for each site and overall to assess the accuracy and uncertainty of the model, along with an analysis of the error distribution. Furthermore, a qualitative visual assessment of the outputs was conducted to determine where the eBTM over- and underestimated the actual flood extent.

3 | Results and Discussion

3.1 | Spatial Modeling Accuracy of the eBTM

For an insight into the magnitude of the observed modeling errors, for all validation points, the distance of the modeled flood line to the actual flood line indicated by the validation points was measured and plotted as a histogram with 3 m classes (Figure 4). The histogram shows that for 188 points out of the total 332 points (56.63%) the modeled flood extent was within a distance of 3.00 m to the nearest validation point. For 57 points (17.17% of points), the distance was between 3.01 and 6.00 m, leading to a total of 73.8% of all points being modeled with a spatial error below 6.00 m. For 53 points (15.96%), the error distance was > 9 m. The average RMSE for all points is 4.88 m.

3.2 | Qualitative Assessment of Results

Table 2 provides a more differentiated picture of the model performance across the eight subsites with the site-specific total number of validation points, RSME, and the percentage and number of points with an error distance below and above the mean RSME of 4.88 m. The table shows that 69.9% of all points have error distances below the mean RSME of 4.88 m, with the percentage of points with error distance below 4.99 m per site ranging between 58.41% and 100%.

For Bloubergstrand, a wave run-up height of 3.3 m was used when running the eBTM and 113 validation points were collected after the storm. Figure 5 shows that for a high number of validation points, the flood extent was drastically underestimated, with 8 points being off between 15 and 22 m which contributed to the high local RSME of 7.61 m. The reason for the underestimation might be the strong easterly winds recorded during the storm which might have pushed the flood water further inland, as those areas indicated in Figure 5 are somewhat funnel shaped.

For Mouille Point (Figure 6), the model was run with a wave run-up of 5.59 m, the highest run-up among all the sites. This part of the coast is highly modified, characterized by a shallow rocky shore and a wide paved/tarred promenade at the water's edge, without a seawall, but with a low (about 1 m) vegetated berm on the landward side of the western stretch of the Sea Point. The berm is interrupted by parking areas and walkways (Figure 6a).

The observed overestimation of the flood extent in this area by up to 22 m, leading to the highest RSME of 8.68 m of all sites, is likely related to modeled water flowing through these gaps and flooding the hinterland and excluded effects of high surface roughness of vegetated areas. Underestimations might be related to the model's omission of wind push.

In the case of the Sea Point site (Figure 7), a wave run-up height of 5.1 m was used as input. Here, the coast is also highly modified, characterized by shallow rocky reef, overlaid with partly wide sandy areas in the nearshore. The water's edge was developed into a wide paved promenade, with an about 1 m high concrete seawall on the seaward side. The seawall ends at the little

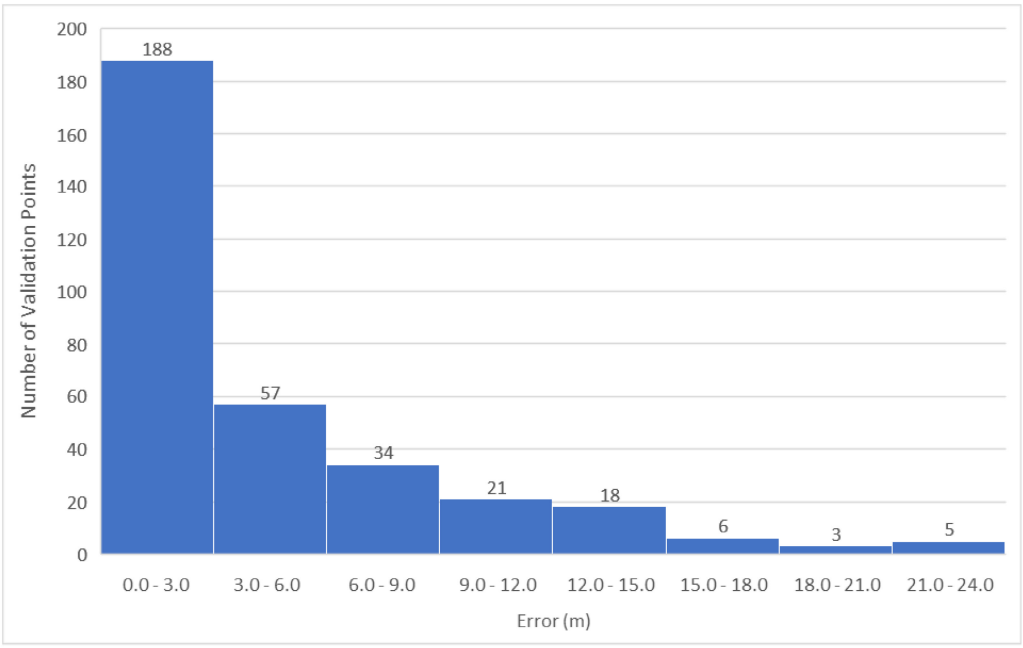

FIGURE 4 | Distance error histogram for all validation points for all subareas.

FIGURE 5 | Modeled flood extent and validation points for Bloubergstrand; (a) areas of underestimation; (b) areas of correct model outputs; (c) areas of under- and overestimation.

beach in the northeastern part of the image. Drastic under- and overestimation of up to 13 m from the recorded flood line took place in this subarea (Figure 7a,b).

The seawall is likely the reason for the high amount of false model outputs, as in parts gaps in the seawall led to (unrealistic extensive) flooding of the hinterland (Figure 7a), while in other

TABLE 2 | Root mean square error (RSME) per site and average, as well as number and percentage of points with error distances below and above the RSME.

No.	Subareas	No of val. points	Subarea RMSE (m)	No. below 4.88 m	No. above 4.88 m	% below 4.88 m
1	Melkbosstrand North	35	6.52	24	11	68.57
2	Melkbosstrand South	40	4.54	33	7	82.50
3	Bloubergstrand	113	7.61	66	47	58.41
4	Lagoon Beach	13	1.04	13	0	100.00
5	Mouille Point	47	8.68	29	18	61.70
6	Sea Point	40	6.07	26	14	65.00
7	Camps Bay	26	3	23	3	88.46
8	Bakoven Beach	18	1.61	18	0	100.00
	Total	332	4.88 (RMSE average)	232 (69.9%)	100 (30.1%)	

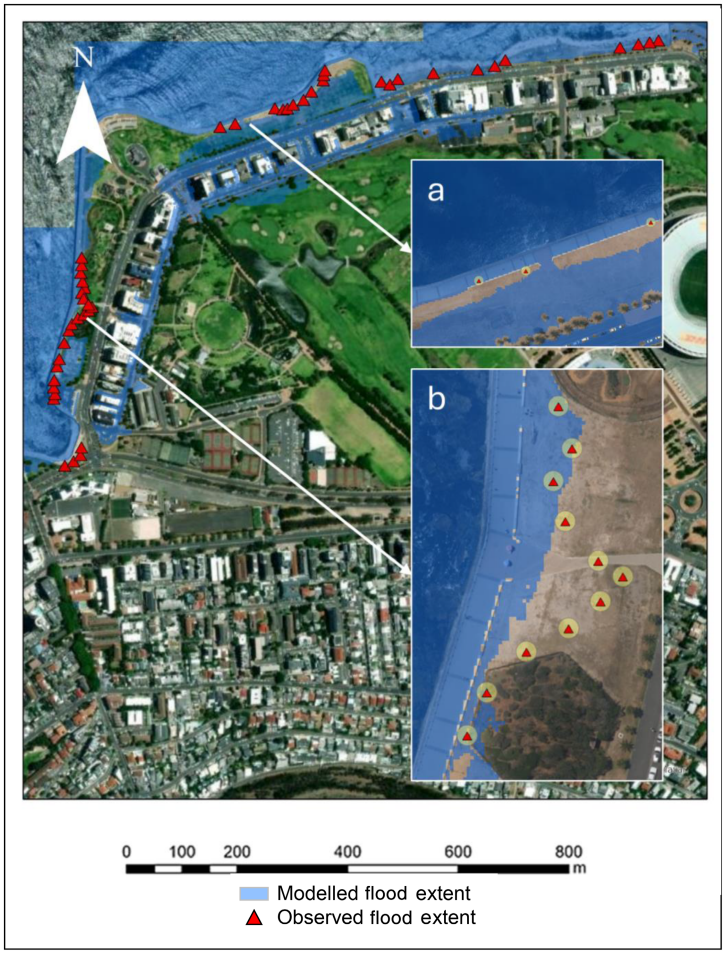

FIGURE 6 | Modeled flood extent and validation points for Mouille Point; (a) areas of overestimation; (b) areas of underestimation.

areas the wetting of the hinterland due to overtopping waves (Figure 7b) was not picked up. The ignored dampening effect of the vegetation and the rocky reefs might have played a role in the overestimation as well.

Figure 8 presents the output for the Bakoven Beach subarea. The residential development in this area is located on a rock shelf that extends 25 to 70 m seawards and protects this otherwise very exposed area from the immediate energy of waves.

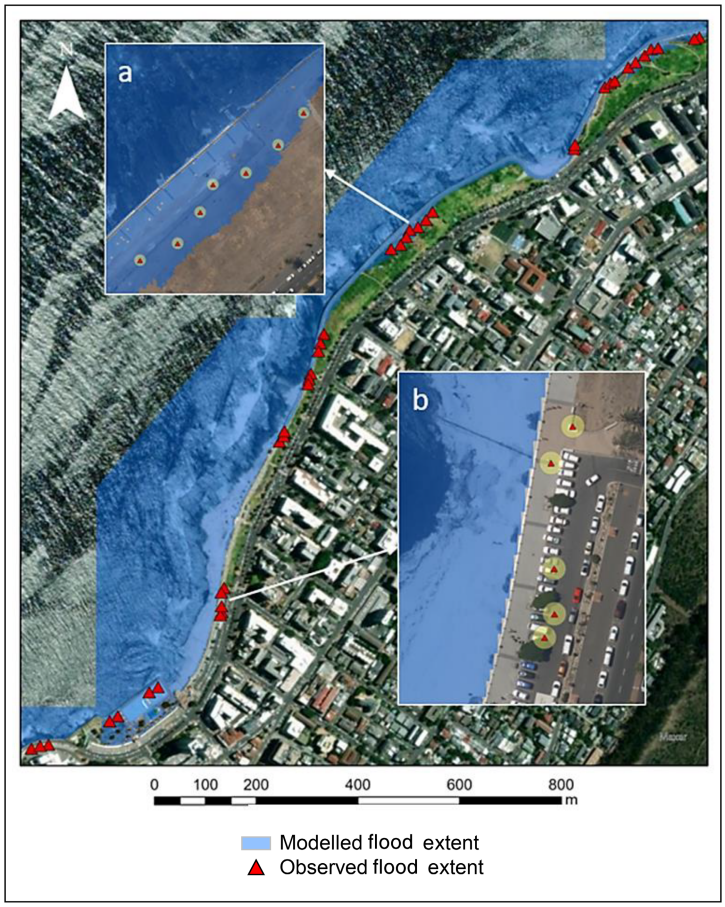

FIGURE 7 | Modeled flood extent and validation points for Sea Point; and validation points and validation points (a) areas of overestimation; (b) areas of underestimation.

Consequently, this area only experienced a wave run-up height of 3.06 m during the investigated storm event. The eBTM produced the most accurate outputs for this sub-area, with an RSME of 1.61 m. The largest error distance in this area was 4.18 m, that is, below the overall RSME of 4.88 m. This indicates that for this area probably factors such as wind push, surface roughness and date of the elevation model were negligible. Potentially, also the small size of this subareas reduces the variability in wave run-up heights, contributing to more precise model predictions than the other subareas.

The modeling outputs for the other subareas are likely to be affected to some extent by the same factors as the four subareas described above, such as the dampening effect of the present vegetation on flood leading to flood overestimation and not considered windpush leading to underestimation. Furthermore, for the northern part of False Bay, only a 2021 DSM was available, which might, particularly for the soft and dynamic coastal stretch in the vicinity of the Sout River estuary (Melkbosstrand North subarea, Appendix B.1), not have reflected accurately the coastal topography at the time of the storm anymore.

Another factor that might have led to overestimation of flood extent is that the eBTM does not consider local nearshore bathymetry and geomorphology. For Melkbosstrand South (Appendix B.2), the flood extent was overestimated by up to 17 m, especially in the area of the parking lot in the south. However, shallow rocky reefs to the south and shallow wide beaches to the north of the parking lot might have dampened the wave run-up.

At Lagoon Beach, the flood extent for all 13 validation points was modeled correctly (Appendix B.3). This site was modeled with a wave run-up height of 3.04 m.

In the case of Camps Bay (Appendix B.4), the model was run with a wave run-up value of 3.04 m. The overall accuracy in this subarea was 77%, where for five validation points out of 26 points the flood extent was underestimated and overestimated for one point. The maximum error distance for this area was 6.8 m.

Further consideration was given to the RMSE relative to the individual site morphology to determine whether there was a general trend in the applicability of the eBTM (Table 3). It appears that for the study sites where intertidal or subtidal reefs are present, the RMSE for the individual sites are above the average (4.88 m). This may indicate that reefs have a dampening effect on the flooding extent that the eBTM cannot account for. Furthermore, the eBTM uses a reference coastline as its starting point, which is landward of these reefs and hence cannot consider their influence. The eBTM may therefore be more applicable to areas where wave propagation is uninterrupted.

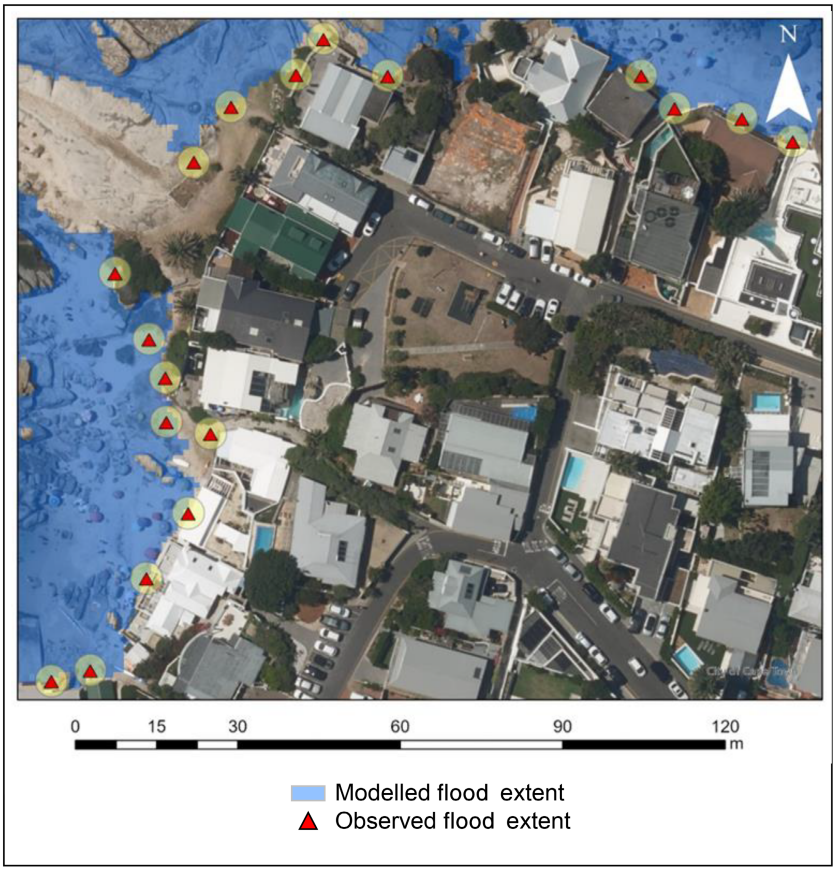

FIGURE 8 | Modeled flood extent and validation points for Bakoven Beach.

TABLE 3 | Study subareas morphology and site-specific RSME.

Study sites	Classification	Local RSME
a Melkbosstrand North	Shallow wide sandy shore + reef	6.52
b Melkbosstrand South	Shallow narrow sandy shore	4.54
c Bloubergstrand	Shallow narrow sandy shore + reef	7.61
d Lagoon Beach	Shallow narrow sandy shore with estuary mouth	1.04
e Mouille Point	Highly modified shore + reef	8.68
f Sea Point	Highly modified shore + reef	6.07
g Camps Bay	Shallow wide sandy shore	3.0
h Bakoven Beach	Steep rocky shore	1.61

4 | Conclusions and Recommendations

This study aimed to establish the robustness of the GIS-based eBTM for storm-related coastal flood modeling. Previously, the eBTM has only been used to model statistical storm and future-dated sea-level rise scenarios which made it impossible to conduct any form of accuracy assessment on the model outputs for the South African coast (DEFF 2020). To circumvent the inherent insecurity of the future-dated input scenario used there, here, we evaluated the eBTM model outputs at eight sites to test against the observed flood extent that occurred in Table Bay, Cape Town, South Africa during a storm event on 16 September 2023. For this storm event, wave run-up, wind direction, and speed, as well as inundation extent were known.

The results show that the eBTM produced flood extents with an RSME of 4.88 m, established using 332 validation points across the eight sites in Table Bay, with 232 points (69.9%) of all validation points having an error distance of < 4.88 m. The RSME for the individual eight test sites ranged between 1.61 and 8.68 m. For 188 points out of the total 332 points (56.63%), the modeled flood line was within 3.0 m to the nearest ground observed flood line. For 57 points (17.17%) the error distance was between 3.01

and 6.0 m, leading to a total of 73.8% of all points being modeled with a spatial error below 6.0 m. For 53 points (15.96%), the error distance was > 9 m, and for 6 points, the error distance was between 20 and 24 m.

Considering the classifications, the higher error distances occurred in areas that had local reefs present, which would dampen wave run-up and serve as natural protection for the receiving environment, notwithstanding that the eBTM is run landward of these reefs.

The results showed that across all 332 validated points in Table Bay the model output accuracy is within an acceptable range. However, at a local-scale, factors such as wind push and overtopping, backflooding and microrelief, nearshore bathymetry, and geomorphology (rocky reefs) led to locally larger error margins in the model outputs. Furthermore, it is likely that microscale wave dissipation dynamics played a role in the observed nonlinear coastal flooding of Table Bay.

The results indicate that the eBTM, which in its current version does not account for the above-mentioned local-scale factors, is best used in subregional applications. The results also show that the use of locally derived wave run-up heights led to an acceptable overall RSME of 4.88 m for the entire Table Bay test area. However, the substantial variation of spatial errors between individual validation points indicates that the eBTM outputs should not be used to inform locally explicit flood adaptation measures, especially if derived, as in our case from one individual storm event.

If no other coastal flood modeling solutions are available to inform coastal spatial planning, disaster preparedness and for climate change adaptation, the results of this study suggest that the application of a buffer on the modeled floodline outputs is advisable to account for the inherent input data insecurities and unaccounted local-scale factors. The achieved local RSME could be used to determine the needed buffer width.

The demonstrated impact of the complexity of the Table Bay coast and the small-scale factors driving coastal flood propagation locally provide valuable insights on the weaknesses of the current eBTM version and on development areas which might improve modeling outputs on a local scale within the limitations of a GIS environment. These could include the consideration of a spatially more differentiated surface roughness, potentially extending into the intertidal area, the duration of the storm as proxy for the total amount of water available for hinterland flooding (to reduce unrealistic flood results of vast hinterland areas), and an emphasized flood propagation direction as proxy for wind direction.

However, local-scale wave data generation primarily relies on hydrodynamic modeling, a process known to be expert-dependent and resource-intensive which currently creates a bottleneck in coastal flood modeling, especially in data and capacity scarce developing countries, such as South Africa, even if GIS tools such as the eBTM itself are easily and freely accessible, albeit based on proprietary software.

In conclusion, the results of this study foster a more comprehensive and evidence-based approach to coastal flood risk assessment, laying the groundwork for improved strategies for safeguarding coastal areas, and enhancing resilience in the face of climate-related risks, although more insights from further local applications of the eBTM are desirable.

Acknowledgments

The core of the presented work was done in the BSc Honors thesis of J. van Voller at Stellenbosch University, Department of Geography & Environmental Studies in 2023 under supervision of M. Lück-Vogel. The Authors would like to thank the South African Geomatics Council for the Bursary for J. van Voller. M. Lück-Vogel's contribution was funded by the South African Parliamentary Grant project P1ECS01.

Conflicts of Interest

The authors declare no conflicts of interest.

Data Availability Statement

The data that support the findings of this study are available from the corresponding author upon reasonable request.

References

Almaliki, A. H., B. Zerouali, C. A. Guimarães Santos, et al. 2023. "Assessing Coastal Vulnerability and Land Use to Sea Level Rise in Jeddah Province." *Kingdom of Saudi Arabia. Heliyon* 9, no. 8: 1–19. https://doi.org/10.1016/j.heliyon.2023.e18508.

Baztan, J., O. Chouinard, B. Jorgensen, P. Tett, J.-P. Vanderlinden, and L. Vasseur. 2015. *Coastal Zones: Solutions for the 21st Century: Introduction*, xxi–xxiii. Elsevier. https://doi.org/10.1016/b978-0-12-802748-6.02001-5.

Bopape, M.-J., G. Keebine, T. Ndarana, et al. 2024. "Weather related disasters in South Africa between 1981 to 2022." In *Presentation at the International Conference on Integrated Responses to the Intensification of Extreme Climate and Weather Events in Developing Economies*, 22–24 May 2024, Stellenbosch, South Africa. https://www.access.ac.za/.

Carneiro-Barros, J. E., T. A. Plomaritis, T. Fazeres-Ferradosa, P. Rosa-Santos, and F. Taveira-Pinto. 2023. "Coastal Flood Mapping With Two Approaches Based on Observations at Furadouro, Northern Portugal." *Remote Sensing* 2023, no. 15: 5215. https://doi.org/10.3390/rs15215215.

Center for International Earth Science Information Network (CIESIN), Columbia University, and CUNY Institute for Demographic Research (CIDR), City University of New York. 2024. *Low Elevation Coastal Zone (LECZ) Global Delta Urban-Rural Population and Land Area Estimates, Version 1*. Palisades, NY: NASA Socioeconomic Data and Applications Center (SEDAC). https://doi.org/10.7927/4hgr-db70.

Clasing, R, E. Muñoz, J. L. Arumí, and V. Parra. 2023. "Remote Sensing with UAVs for Flood Modeling: A Validation with Actual Flood Records." *Water* 15: 3813. https://doi.org/10.3390/w15213813.

Crossland, C. J., H. H. Kremer, H. J. Lindeboom, J. I. Marshall Crossland, and M. D. A. Le Tissier, eds. 2005. *Coastal Fluxes in the Anthropocene: The Land–Ocean Interactions in the Coastal Zone. Project on the International Geosphere-Biosphere Programme Series. Global Change: The IGBP Series*. Berlin, Heidelberg: Springer-Verlag.

Department of Environment, Forestry & Fisheries. 2020. *National Coastal Climate Change Vulnerability Assessment: Vulnerability Indices* [Technical Report]. Pretoria, South Africa.

Dube, K., G. Nhamo, and D. Chikodzi. 2022. "Flooding Trends and Their Impacts on Coastal Communities of Western Cape Province, South Africa." *GeoJournal* 87, no. S4: 453–468. https://doi.org/10.1007/s10708-021-10460-z.

Fitchett, J. M., B. Grant, and G. Hoogendoom. 2016. "Climate Change Threats to Low-Lying South African Coastal Towns: Risks and Perceptions." *South African Journal of Science* 112, no. 5/8: 1–9. https://doi.org/10.17159/sajs.2016/20150262.

Gesch, D. B. 2009. "Analysis of Lidar Elevation Data for Improved Identification and Delineation of Lands Vulnerable to Sea-Level Rise." *Journal of Coastal Research* 10053: 49–58. https://doi.org/10.2112/SI53-006.1.

Goschen, W. 2011. *Coping With Sea Level Rise and Storm Surges*. SAEON. http://archive.saeon.ac.za/enewsleter-archives/2011/april2011/doc08.

Intergovernmental Panel on Climate Change. 2019. "Summary for Policymakers." In *IPCC Special Report on the Ocean and Cryosphere in a Changing Climate*, edited by H.-O. Pörtner, D. C. Roberts, and V. Masson-Delmotte, 3–35. Cambridge: Cambridge University Press. https://doi.org/10.1017/9781009157964.001.

Intergovernmental Panel on Climate Change. 2021. *The Physical Science Basis: Contribution of Working Group I to the Sixth Assessment Report of the Intergovernmental Panel on Climate Change*, edited by V. Masson-Delmotte, P. Zhai, and A. Pirani, eds. Cambridge: Cambridge University Press. https://doi.org/10.1017/9781009157896.001.

Intergovernmental Panel on Climate Change. 2022. "Cross-Chapter Paper 2: Cities and Settlements by the Sea." In *Climate Change 2022: Impacts, Adaptation and Vulnerability. Contribution of Working Group II to the Sixth Assessment Report of the Intergovernmental Panel on Climate Change*, edited by B. C. Glavovic, R. Dawson, and W. Chow, 2163–2194. Cambridge: Cambridge University Press. https://doi.org/10.1017/9781009325844.019.

Jennath, A., and S. Paul. 2024. "A Multi-Risk Approach for Projecting Climate Change-Associated Coastal Flood, Applied to India." *Natural Hazards* 120: 4581–4600. https://doi.org/10.1007/s11069-024-06420-8.

Kouakou, M., J. A. Tiémélé, E. Djagoua, and K. Gnandi. 2023. "Assessing Potential Coastal Flood Exposure Along the Port-Bouët Bay in Côte D'ivoire Using the Enhanced Bathtub Model." *Environmental Research Communications* 5: 10. https://doi.org/10.1088/2515-7620/acfdfa.

Li, X., C. J. Grady, and A. Peterson. 2014. "Delineating Sea Level Rise Inundation Using a Graph Traversal Algorithm." *Marine Geodesy* 37: 267–281. https://doi.org/10.1080/01490419.2014.902884, https://www.researchgate.net/publication/262774465_Delineating_Sea_Level_Rise_Inundation_Using_a_Graph_Traversal_Algorithm.

Nguyen, J., and Y. Kuleshov. 2023. "Coastal Inundation Hazard Assessment in Australian Tropical Cyclone Prone Regions." *Hydrology* 10, no. 12: 228. https://doi.org/10.3390/hydrology10120228.

Quinn, N., M. Lewis, M. P. Wadey, and I. D. Haigh. 2014. "Assessing the Temporal Variability in Extreme Storm-Tide Time Series for Coastal Flood Risk Assessment." *Journal of Geophysical Research, Oceans* 119: 4983–4998. https://doi.org/10.1002/2014JC010197.

Rohmer, J., D. Lincke, J. Hinkel, G. Le Cozannet, E. Lambert, and A. T. Vafeidis. 2021. "Unravelling the Importance of Uncertainties in Global-Scale Coastal Flood Risk Assessments Under Sea Level Rise." *Water* 13: 774. https://doi.org/10.3390/w13060774.

Roux, A. P. 2015. *A Re-Assessment of Wave Run Up Formulae* [Thesis]. Stellenbosch University.

Rutledge, K., M. McDaniel, S. Teng, et al. 2022. *Coast. In Earth Science, Geology, Oceanography, Geography, Physical Geography*. Washington, DC: National Geographic Society. https://education.nationalgeographic.org/resource/coast/.

Saravanan, S., K. S. S. Parthasarathy, and S. R. Vishnuprasath. 2019. "Chapter 4—Monitoring Spatial and Temporal Scales of Shoreline Changes in the Cuddalore Region, India." In *Coastal Zone Management*, 99–112. Amsterdam: Elsevier. https://doi.org/10.1016/b978-0-12-814350-6.00004-5.

Sink, K. J., S. Holness, L. Harris, et al. 2012. *National Biodiversity Assessment 2011: Technical Report. Volume 4: Marine and Coastal Component*. South African National Biodiversity Institute.

Skowno, A. L., C. J. Poole, D. C. Raimondo, et al. 2019. *National Biodiversity Assessment 2018: The Status of South Africa's Ecosystems and Biodiversity*. Synthesis Report, 1–214. South African National Biodiversity Institute, an Entity of the Department of Environment, Forestry and Fisheries, Pretoria. https://www.sanbi.org/wp-content/uploads/2019/10/NBA-Report-2019.pdf.

Theron, A., and M. Rossouw. 2008. "Analysis of Potential Coastal Zone Climate Change Impacts and Possible Response Options in the Southern African Region." In *Proceedings of the Science Real and Relevant: 2nd CSIR Biennial Conference*. Pretoria: CSIR International Convention Centre. http://hdl.handle.net/10204/2561.

United Nations. 2016. *Atlas of the Oceans*. http://www.oceansatlas.org/subtopic/en/c/114/.

Vousdoukas, M., D. Bouziotas, A. Giardino, et al. 2018. "Understanding Epistemic Uncertainty in Large-Scale Coastal Flood Risk Assessment for Present and Future Climates." *Natural Hazards and Earth System Sciences* 18: 2127–2142. https://doi.org/10.5194/nhess-18-2127-2018.

Wepener, V., and N. Degger. 2019. "South Africa." In *World Seas: An Environmental Evaluation*, edited by C. Sheppard, 2nd ed., 101–119. Cambridge, MA: Academic Press. https://doi.org/10.1016/b978-0-08-100853-9.00006-3.

Williams, L. L. 2020. *Developing a Spatial Risk Profile: Assessing Building Vulnerability to Extreme Coastal Inundation Hazard* [Unpublished thesis]. Stellenbosch University.

Williams, L. L., and M. Lück-Vogel. 2020. "Comparative Assessment of the GIS Based Bathtub Model and an Enhanced Bathtub Model for Coastal Inundation." *Journal of Coastal Conservation* 24: 23. https://doi.org/10.1007/s11852-020-00735-x.

Williams, L. L., and M. Lück-Vogel. 2022. "Geographic Information System Data Considerations in the Context of the Enhanced Bathtub Model for Coastal Inundation." *Transactions in GIS* 26: 3074–3089. https://doi.org/10.1111/tgis.12995.

Williams, S. J., K. Dodd, and K. K. Gohn. 1995. *Coasts in Crisis*. US Geological Survey. Washington, DC: US Department of the Interior.

Appendix A | **Description and Classification of the Study Subareas.**

Study subareas	Site description	Classification	Image (source: Google Earth)
a Melkbosstrand North	Shallow sandy shore with vegetated dunes and small estuary, has a parking area next to the small estuary with a few small trails connecting it to the beach. A prominent subtidal reef is present in the central site area	Shallow, wide (> 50 m) sandy shore with small reef	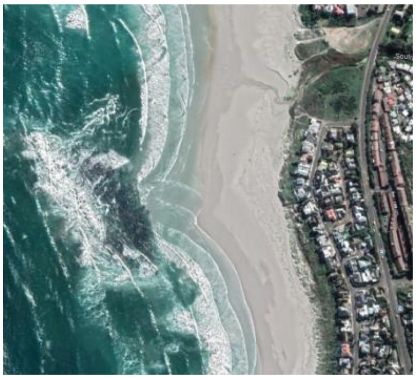
b Melkbosstrand South	Shallow sandy shore with interspersed vegetated dunes and grassy hinterland, confined by road infrastructure. The far south coastline has a flat rocky substrate	Shallow, narrow (< 50 m) sandy shore, partially with reef	
c Bloubergstrand	Rocky shoreline interspersed with sandy patches and featuring intertidal and subtidal reefs, adjacent to Bloubergstrand's residential area. The coast is lined with rugged rocks, particularly prominent in the north, transitioning to long sandy beaches with vegetated dunes to the north and dune rehabilitation areas to the south. A small break wall is visible behind the rocky beaches where houses are close to the waterline	Shallow, narrow (< 50 m) sandy shore + reef	
d Lagoon Beach	Curved sandy shoreline with a small estuary, partly stabilized with revetments. Behind the revetments, there is a walking path with another wall directly behind it, leading to a narrow grassy recreational area. The area is mostly confined by residential development in the hinterland, with the beach easily accessible from the modern coastal complex	Shallow, narrow (< 50 m) sandy shore with estuary mouth	

(Continues)

Appendix A | (Continued)

Study subareas	Site description	Classification	Image (source: Google Earth)
e Mouille point	Rocky coastline featuring intertidal reefs with a concrete promenade and a low seawall along the shore. The area features a narrow grassy strip and a walking path, with residential and commercial buildings lining the road that runs parallel to the promenade	Highly modified, narrow (< 50 m) shore + reef	
f Sea point	Rocky coastline featuring a concrete promenade with a low seawall along a rocky shore, interspersed with small sandy pocket beaches. The promenade runs parallel to a major road and is bordered by a grassy recreational area on the inland side, with parking areas and outdoor swimming pools directly bordering the seawall. The rocky shoreline bears both subtidal and intertidal reefs and transitions to these sandy pockets further along the coast	Highly modified, narrow (< 50 m) shore + reef	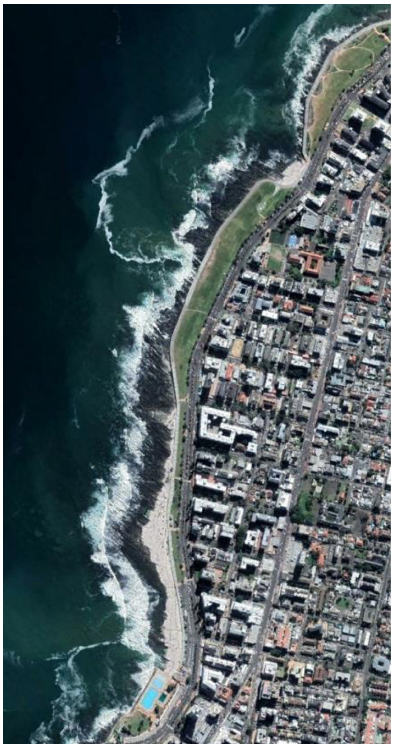
g Camps Bay	Wide sandy beach with a steep slope toward the vegetated dunes, transitioning into a grassy recreational belt, with a road running parallel to the beach	Shallow, wide (> 50 m) sandy shore	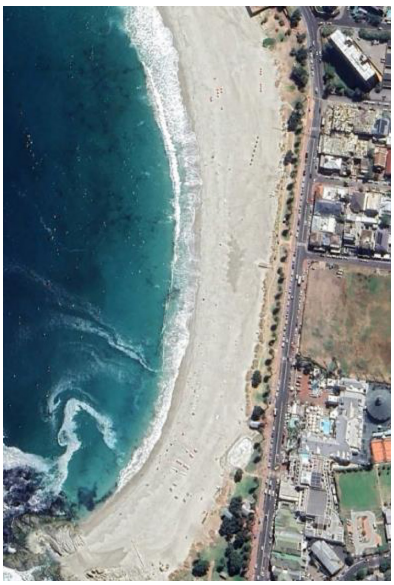

(Continues)

Appendix A | (Continued)

Study subareas	Site description	Classification	Image (source: Google Earth)
h Bakoven Beach	Rocky coastline with small sandy coves at Bakoven and Beta Beach, characterized by large granite boulders and a wide rock shelf that extends 25 to 70 m seaward. This rock shelf not only provides some natural protection but also directs wave energy toward the shore	Steep, wide (> 50 m) rocky shore	

Appendix B | **Maps of Subarea Flood Modeling Results Not Discussed in Detail in the Text.**

B.1 | Melkbosstrand North

Modeled flood extent and validation points for Melkbosstrand North; (a) Areas of overestimated flood extent; (b) Areas of over- and underestimation.

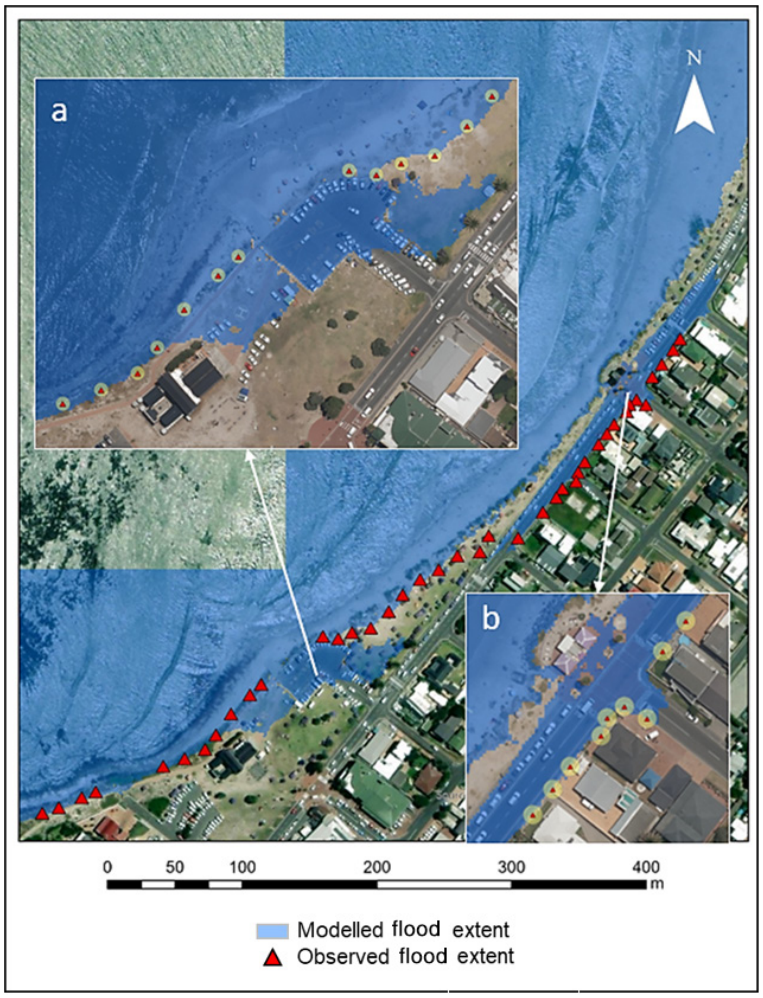

Modeled flood extent and validation points for Melkbosstrand South; (a) Areas of overestimated flood extent: (B) Areas of correct model outputs.

Modeled flood extent and validation points for Lagoon Beach; (a) Detail of modeled flood extent result.

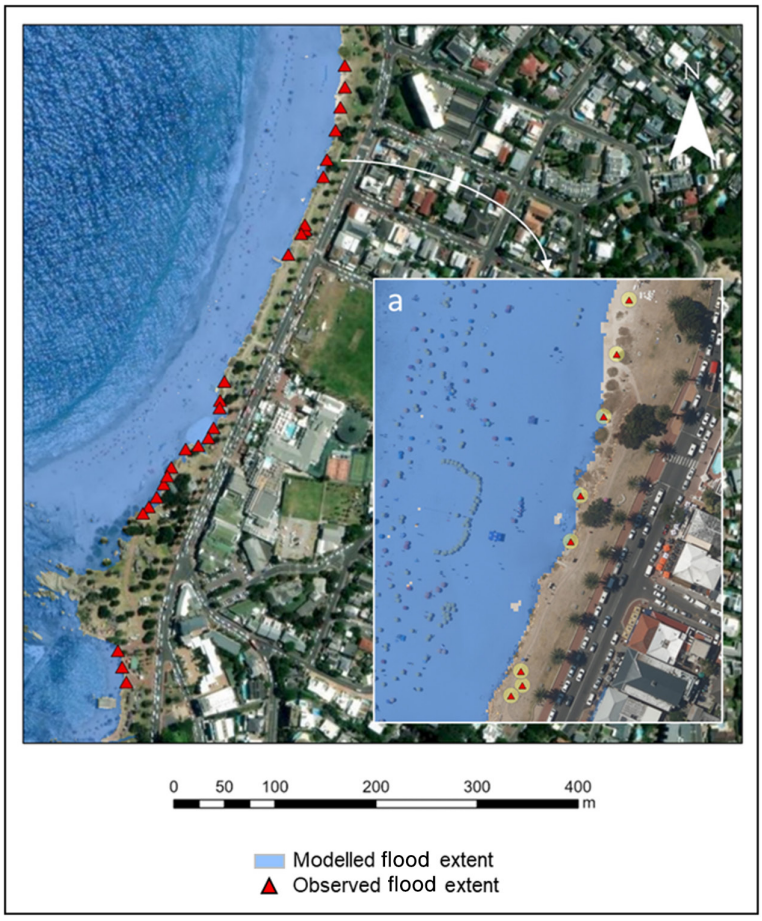

Modeled flood extent and validation points for Camps Bay; (a) Area where modeling errors occurred.